INL/JOU-20-59957-Revision-0

Transient testing of uranium silicide fuel in zircaloy and silicon carbide cladding

September 2021

David W Kamerman, Nicolas E Woolstenhulme, Devin D Imholte, Austin D Fleming, Colby B Jensen, Charles P Folsom, Connor T Woolum, Korbin E Tritthart, Jason L Schulthess, Daniel M Wachs

Changing the World's Energy Future

INL is a U.S. Department of Energy National Laboratory operated by Battelle Energy Alliance, LLC

INL/JOU-20-59957-Revision-0

Transient testing of uranium silicide fuel in zircaloy and silicon carbide cladding

David W Kamerman, Nicolas E Woolstenhulme, Devin D Imholte, Austin D Fleming, Colby B Jensen, Charles P Folsom, Connor T Woolum, Korbin E Tritthart, Jason L Schulthess, Daniel M Wachs

September 2021

Idaho National Laboratory
Idaho Falls, Idaho 83415

http://www.inl.gov

Prepared for the
U.S. Department of Energy
Under DOE Idaho Operations Office
Contract DE-AC07-05ID14517

Transient Testing of Uranium Silicide Fuel in Zircaloy and Silicon Carbide Cladding

David Kamerman – ORCID: 0000-0002-2610-038X – David.Kamerman@inl.gov

Nicolas Woolstenhulme – ORCID: 0000-0002-7881-3314 – Nicolas.Woolstenhulme@inl.gov

Devin Imholte – ORCID: 0000-0001-8415-0409 – Devin.Imholte@inl.gov

Austin Fleming – ORCID: 0000-0002-6801-5028 – Austin.Fleming@inl.gov

Colby Jensen – ORCID: 0000-0001-8925-7758 – Colby.Jensen@inl.gov

Charles Folsom – ORCID: 0000-0002-8242-8777 – Charles.Folsom@inl.gov

Connor Woolum– Connor.Woolum@inl.gov

Korbin Tritthart– Korbin.Tritthart@inl.gov

Jason Schulthess – ORCID: 0000-0002-4289-7528 – Jason.Schulthess@inl.gov

Dan Wachs – ORCID: 0000-0002-9239-3424 – Daniel.Wachs@inl.gov

Idaho National Laboratory, 2525 N. Fremont Ave, Idaho Falls, Idaho 83415

Corresponding Author:

David Kamerman

Idaho National Laboratory, 2525 N. Fremont Ave,

P.O. Box 1625, MS 3840, Idaho Falls, Idaho 83415

Phone: (208) 270-3321, Email: David.Kamerman@INL.gov

Abstract –

Using the newly restarted Transient Reactor Test (TREAT) facility at Idaho National Laboratories, fresh (unirradiated) U_3Si_2 fuel pellets were tested under reactivity-initiated accident conditions in dry helium capsules. These tests were performed with total energy depositions sufficient to induce melting of the U_3Si_2 fuel pellets based on available thermophysical property data. The instrumented experiments utilized in-pile thermocouples and infrared pyrometers to measure the cladding temperature during the transient, which are in reasonable agreement with predicted peak cladding temperatures using a simple BISON fuel performance model. This same model is then used to predict expected cladding stresses during the transients in areas where pellet cladding interaction is expected. It was shown that for transient energy depositions up to 528 J/g rod like geometry of the test articles was maintained. While it is acknowledged that more confirmatory testing is required in more prototypic environments, these first of their kind experiments have demonstrated that unirradiated U_3Si_2 fuel and unirradiated SiC-SiC claddings can likely retain a "rod like" geometry for transient energy depositions up to 528 J/g.

Keywords – Nuclear Fuel Safety Research, Irradiation Testing, Irradiation Environment, Nuclear Testing, Transient Testing, Uranium Silicide, Silicon Carbide.

1 Introduction

Following the tragic events at Japan's Fukushima Daiichi power plant in 2011, priority was given within the United States (U.S.) Department of Energy (DOE)-sponsored research programs in advanced nuclear fuels was given to increasing the accident tolerance of fuel systems for light water reactors (LWRs) [1]. These enhanced accident tolerant fuel (ATF) concepts include a wide variety of fuel and cladding materials, both as variants of the current zircaloy-UO_2 system and as novel fuel and cladding concepts, such as uranium silicide (U_3Si_2) fuel and silicon carbide composite (SiC-SiC) cladding. Monolithic U_3Si_2 fuel pellets have recently shown excellent fission gas retention, limited swelling, and limited cracking after being irradiated to around 20 MWd/kgU [2]. However, recent studies have also showed that reactions with pressurized water coolant could prove problematic and lead to washout behavior in breeched rods [3][4]. SiC-SiC claddings are generally comprised of wound nuclear grade SiC fibers embedded in a SiC matrix [5][6]. The composite material is often paired with other ceramic or metallic inter or outer layers to aid in corrosion resistance and to arrest microcracks [7][8][9]. Integral fuel performance assessments using the BISON [10] and a modified FRAPCON [11] code have evaluated the performance of U_3Si_2 fuel and Silicon Carbide Cladding in prototypic LWR conditions and overpower transients and shown that within certain design constraints, acceptable performance can be achieved. However, as shown in the referenced analysis, fuel rods comprised of U_3Si_2 fuel and SiC-SiC cladding will likely behave very differently in accident conditions requiring the development of new fuel safety criteria to regulate their performance. One of the most challenging design basis accidents (DBAs) for LWRs are rapid high-power excursions that are known as reactivity initiated accidents (RIAs). In pressurized water reactors (PWRs), the design basis RIA is the control rod ejection accident (CREA). In boiling water reactors (BWRs), the design basis RIA is the control rod drop accident

(CRDA). CREAs and CRDAs can result in the insertion of a prompt amount of reactivity, sending the reactor on a rapid positive power period. The power excursions initiated by the CREA/CRDA are terminated as the fuel heats up, and doppler broadening in the fuel decreases the excess reactivity. The resulting power pulse is nominally Gaussian in shape and the width can be characterized by a full width at half maximum (FWHM) or pulse width. For PWRs at hot coolant conditions and zero or low reactor power (such as the case just prior to startup) termed hot zero power (HZP), pulse widths range from 25–65 milliseconds (ms). For BWRs at cold zero power (CZP), the pulse widths range from 45–75 ms [12].

Testing new fuel concepts in RIA transients requires dedicated test reactors capable of simulating these kinds of prompt Gaussian transients. Several such reactors exist around the world, including the Nuclear Safety Research Reactor (NSRR) in Japan [13], CABRI reactor in France [14], and Impulse Graphite Reactor (IGR) in Kazakhstan. In the U.S., several reactors were built and operated specifically for the study of nuclear fuels in transient conditions, including the Transient Reactor Test (TREAT) facility located at Idaho National Laboratory (INL), the Special Power Excursion Reactor Test (SPERT) Program [15], and the Power Burst Facility (PBF) reactor [16]. The TREAT reactor was the first to be built and came online in 1959. It was also the last to be shut down in 1994. Following the resurgence of interest in ATF, the decision was made to restart the TREAT reactor, which was officially brought back online in 2017 [17]. A number of experimental test trains are being developed for testing ATF in TREAT [18], and the first transients with LWR fuel were completed in 2018. These first transients were on standard UO_2 fuel in zircaloy cladding with the purpose of developing the required core to specimen energy coupling coefficients [19][20]. Following these transients, testing on ATF concepts began in 2019, which are the subject of this paper.

2 Materials and Methods

The first ATF concepts to be investigated in TREAT are U_3Si_2 in zircaloy cladding and U_3Si_2 in SiC-SiC cladding. The zircaloy clad tests were planned to partially and significantly melt the fuel and evaluate the effects of the molten fuel interaction with the zircaloy cladding and to determine if a coolable rod geometry could be maintained past the melting point of the fuel. The SiC-SiC clad tests were also planned to significantly melt the fuel to evaluate effects of molten fuel interaction with SiC-SiC cladding as well as to evaluate the integrity of the SiC-SiC cladding when subjected to limited pellet cladding interaction (PCI) prior to fuel melting.

The U_3Si_2 fuel pellets were fabricated at INL using a cold press and sinter method [21][22], the zircaloy cladding was procured commercially, and the SiC-SiC cladding was fabricated by General Atomics [23]. These materials were chosen for initial study as they are thought to be the most challenged by RIA conditions. U_3Si_2 has dramatically different thermal-physical properties from UO_2 [24][25][26] The melting point is much lower (e.g., 1938 K vs 3120 K) as is the high temperature heat capacity (215 J/kg-K at 1000°K vs 312 J/kg-K for UO_2). The thermal conductivity, however, is much higher (23 W/m-K at 1000°K vs 5 W/m-K for UO_2). The lower heat capacity and lower melting point indicate that the likelihood of fuel melting is significantly increased with this fuel type, even for transients with low energy depositions. The enthalpy rise needed to induce melting in the U_3Si_2 fuel can be determined by integrating the heat capacities through the melting temperature which is determined to be approximately 350 J/g-U_3Si_2 pellet enthalpy. To the authors knowledge the heat of fusion for U_3Si_2 has not been published, as such it is unclear how extensive fuel melting may be for enthalpy additions only slightly above this value. The pellet enthalpy and temperature relationship for U_3Si_2 compared with UO_2 is shown in Figure 1.

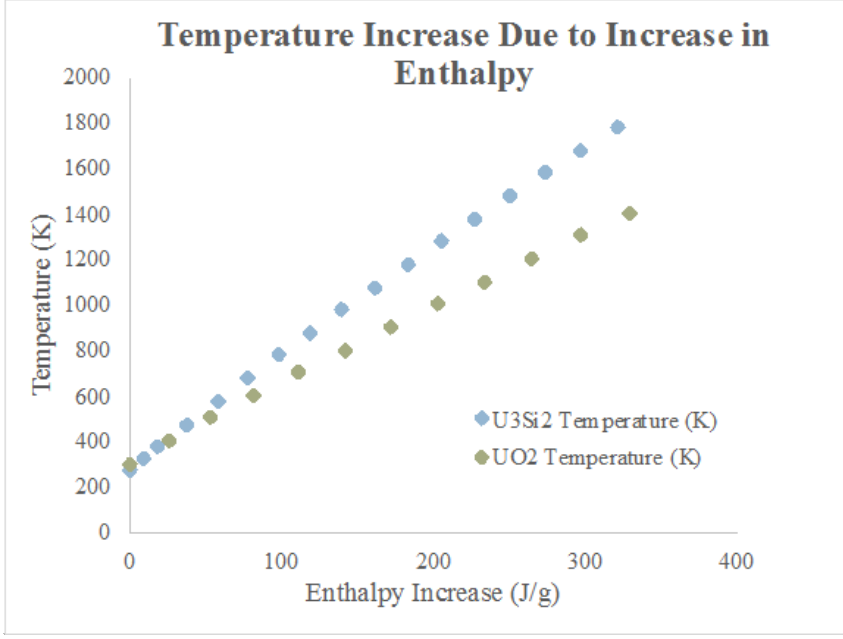

Figure 1. Comparison of UO_2 [14] and U_3Si_2 [15] temperature increase in response to an increase in specific enthalpy.

The thermal expansion coefficient for U_3Si_2 is weakly dependent on temperature and is relatively constant around 15e-6 K^{-1}. Combining the values of thermal expansion with heat capacity for a given transient enthalpy rise shows that significantly more thermal expansion is expected to occur with U_3Si_2 when compared with UO_2, as shown in Figure 2. This increased thermal expansion will lead to more aggressive pellet cladding interactions for a given energy deposition. While the increased thermal conductivity and uranium loading of U_3Si_2 fuel have many potential benefits in normal operations and in other accident scenarios, there are significant challenges for this concept in RIA transients.

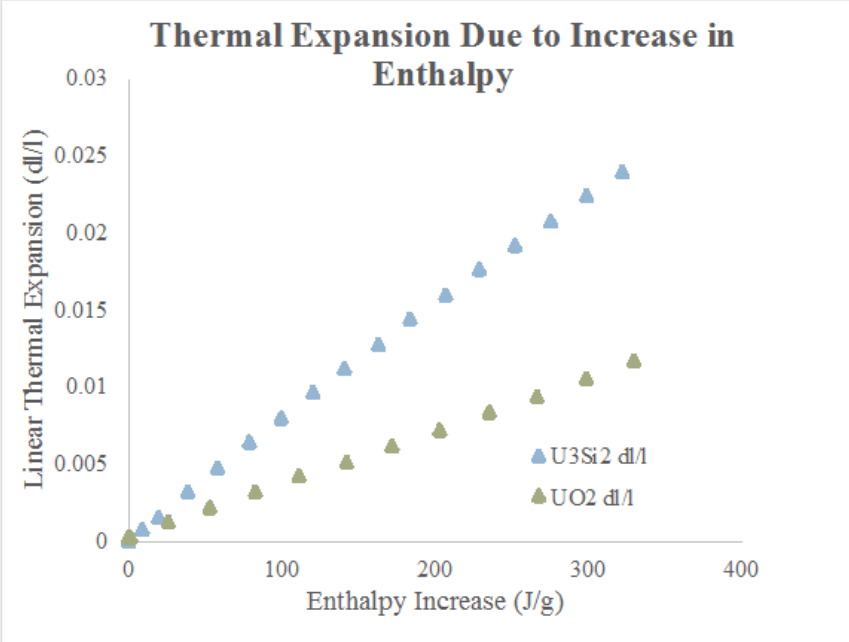

*Figure **2**. Comparison of UO_2 [14] and U_3Si_2 [15] thermal expansion in response to an increase in specific enthalpy.*

SiC-SiC composite cladding has significantly different mechanical behavior than zircaloy metal, which may also impact the performance of this fuel concept in RIAs. While zircaloy is relatively strong at lower temperature (e.g., yield stress ~700MPa in the hoop direction [27]), this strength quickly diminishes at higher temperatures and nearly vanishes above the alpha to beta transition temperature of approximately 800°C. However, the material is highly ductile at both room temperature and elevated temperatures with failure strains ranging from 15–55% depending on heat treatment, temperature, and extent of material degradation due to fast neutron fluence and hydrogen uptake. SiC ceramic materials have near zero ductility, however SiC-SiC composite materials have an extended load carrying capacity behavior defined by a proportional limit stress (analogous to yield stress) and an ultimate tensile stress [28]. In the hoop direction, the proportional limit stress is approximately 150 MPa, while the ultimate tensile stress is approximately 350 MPa. These values do not change appreciably with temperature or irradiation

fluence. However, the material does experience rapid degradation in thermal conductivity in the presence of a fast neutron flux [29]. Significant swelling of the material also occurs as a result of the fast neutron flux up to saturation values near 1 dpa with swelling being greater at lower irradiation temperatures [30]. This cladding material is most vulnerable to displacement-controlled loadings, such as those that occur in the pellet cladding interaction (PCI) phase of an RIA transient. Recent work by Cinbiz et al showed major axial crack formation at low hoop strains (0.5%) in modified burst tests which simulate rapid PCI loadings in RIA transients [31]. The extent of PCI loading during the RIA will depend greatly on the pellet cladding gap size at the time of the transient which will be affected by both the fuel and cladding's irradiation history [32].

2.1 Experiment Fabrication and Assembly

Four rodlets with typical 17x17 PWR radial dimensions (e.g., cladding outside diameter equal to 9.5 mm) where constructed for transient testing. All of the rodlets contained naturally enriched U_3Si_2 fuel to 94% theoretical density. Two rodlets were clad with Zircaloy-4 cladding with a nominal wall thickness of 0.57 mm, and two rodlets were clad with SiC-SiC cladding with a nominal wall thickness of 0.8mm. All four rodlets were approximately 15 cm long with an approximate 10 cm stack of 10 fuel pellets and backfilled with helium at atmospheric pressure. The two rodlets with SiC-SiC cladding contained U_3Si_2 pellets of two diameters resulting in different pellet cladding gaps. The rodlet with the larger and smaller gap were intended to be more prone to failure by fuel melt and PCI, respectively. The rodlets were named following the nomenclature from earlier tests with UO_2 and zircaloy in the Separate Effects Test Holder (SETH)—SETH-F, SETH-G, SETH-H, and SETH-I. Table 1 describes the radial gap size associated with each rodlet.

Table 1. TREAT ATF rodlet materials and gap geometry.

Rodlet	Pellet	Cladding	Nominal Gap (μm)
SETH F	NE-U_3Si_2	Zircaloy – 4	65
SETH G	NE-U_3Si_2	Zircaloy – 4	65
SETH H	NE-U_3Si_2	SiC-SiC	80
SETH I	NE-U_3Si_2	SiC-SiC	50

Fuel rod assembly generally starts with a bottom end plug attachment to the cladding, followed by internals loading, and then the top end plug attachment. Laser welding was selected for securing the end plugs of the zircaloy-4 clad rodlet and a high-temperature ceramic epoxy was used to join the end plugs for the SiC clad rodlet. Assembly of a SiC clad rodlet varies from that of a metal-clad rodlet given the joining processes required for a ceramic base. Commercially, SiC joining and sealing processes are extremely specialized processes utilizing purpose-built equipment in order to form a hermetic seal. As the primary purpose of this irradiation test was to irradiate U_3Si_2 fuel within a SiC-SiC cladding tube rather than test any SiC joint [33], end plugs were affixed into place using Cotronics 989, a high-temperature alumina epoxy demonstrated to be suitable for this application. As the rodlet atmosphere was required to be helium, the SiC-SiC rodlet had to be assembled within a helium atmosphere glovebox.

Instruments included thermocouples and noncontact optical fibers for measurement of the cladding temperature during the transient. In order for the thermocouple's temperature measurements to be accurate, good thermal contact with the fuel rodlet was required. This was achieved in different ways for the SiC and the Zr-4 cladding. In the case of Zr-4 cladding, a tack welding process was developed to weld the thermocouples (Ti-sheath) to the Zr-4 cladding surface. For the SETH-F capsule, two thermocouples were configured to be perpendicular to the

cladding with the other two thermocouples para-axial to the cladding. This configuration, in conjunction with the optical fiber data, could inform which specific thermocouple configuration could provide the most accurate data. The Ti-sheathed thermocouples could not be affixed to SiC cladding using the same process as the Zr-4 cladding. Additionally, as a first-of-a-kind effort, responsiveness of the thermocouples and its dependency on configuration and attachment method was unknown. Various configurations of aluminum wire and a high-temperature epoxy were used to fix the thermocouples into place. The four thermocouples were fixed adjacent to the third, fifth, sixth, and eighth pellets from the bottom in the rodlet. The standard type K thermocouples have a measurement uncertainty of 0.75% of the measurement in the applicable range with a data acquisition uncertainty of 0.77°C, dwarfed by the former error in the temperature range of interest for this work. However, the thermal contact resistance between the thermocouple and cladding surface contribute additional uncertainty during the transient measurement. In this case, the thermocouple is mounted to the surface using epoxy and surrounded by an inert gas, limiting heat losses such that the thermocouple will closely reach the peak cladding temperature. However thermal resistance to the TC junction will contribute to a small time delay in the measured temperature. The delay results in some additional heat losses and undermeasured peak value. The peak temperature values will be more accurately captured by the pyrometer. Therefore, thermocouple measurement can be compared with the pyrometer for an estimate on the expected negative temperature bias in the thermocouple measurements.

The collected light from the optical fibers was analyzed using a custom multi-spectral pyrometry technique. This technique was necessary for data interpretation to account for the radiation-induced emission (e.g., radioluminescence and Cherenkov radiation) in the fiber. Previous laboratory testing and preliminary in-pile tests of this pyrometry system were conducted in preparation of the SETH experiment series [34]. The distal end of the optical fibers

(e.g., core/cladding diameters of 600/660 μm) were polished at a 45-degree angle and oriented so that the axis of the fibers was parallel to the rodlet and tip of the polished angle was oriented towards the rodlet. This ensured that light coming through the side of the fiber and reflecting off the angle polish would propagate through the optical fiber. The two fibers were positioned so that they collected light from the same axial location on the rodlet (between pellets 5 and 6), but at slightly different azimuthal locations. Location of the thermocouples and light fibers is shown in Figure 3. Measurement uncertainties for the pyrometer measurements at the peak temperatures are calculated based on the data reduction scheme to be less than +/- 25°C. This value varies across the span of measured temperatures up to +/- 50°C. The multi-spectral pyrometry technique used in these measurements makes a grey body assumption on the target emissivity. For accurate temperature measurements this is assumption is only required to be satisfied over the spectral range used for the measurement 1000 -1700 nm. From literature, this is assumption is satisfied for both zircaloy and silicon carbide [35]]36].

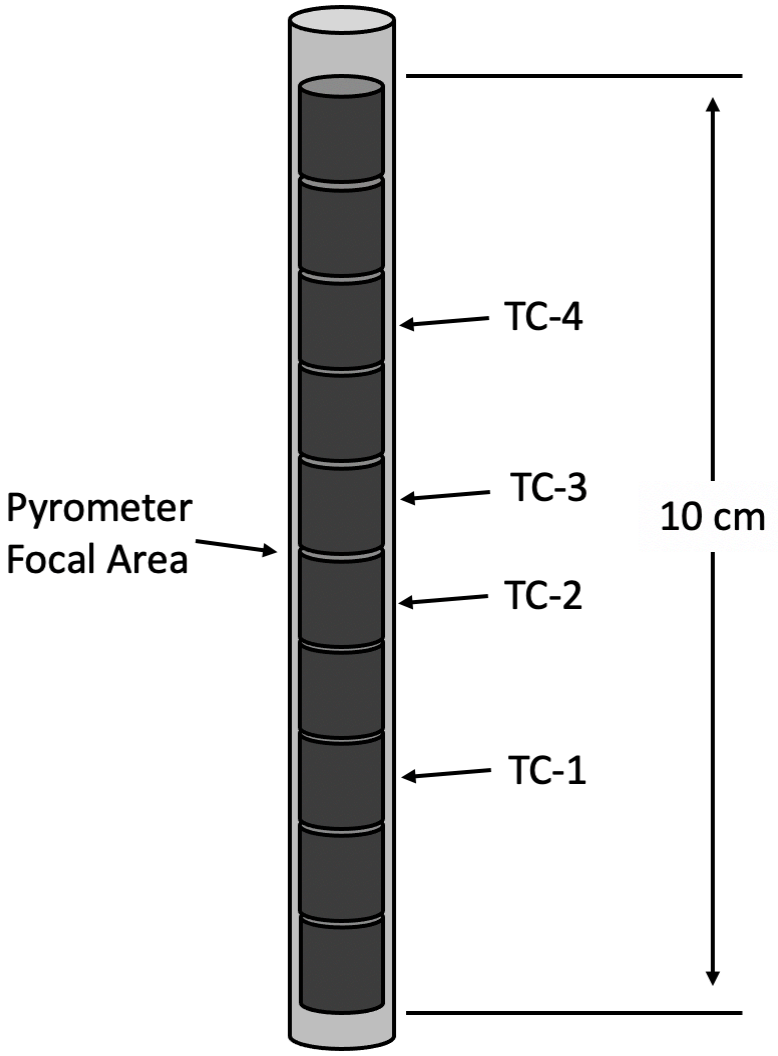

Figure 3) Cladding Temperature Measurement Locations

The rodlets were then loaded into the a static helium-filled capsule [37]. These capsules contained the fabricated rodlets, the instrumentation holders with mounted temperature instruments, and high temperature ceramic melt catchers lining the bottom of the capsules. The capsule assemblies were then inserted into a secondary outer irradiation containment assembly. While the test capsule's helium environment is not prototypic of an LWR operating environment it is conservative when considering rod melting as a failure mode as is the case in the first three tests. As the mechanical (strength) properties of SiC-SiC cladding do not change appreciably

with temperature, the helium capsule environment is also suitable for a first order evaluation of PCI failure of this cladding.

2.2 Transient Irradiation

Transient irradiations took place in the TREAT reactor which is an air-cooled reactor driven by a core of graphite blocks having a small concentration of dispersed uranium dioxide [38]. The irradiation assembly described above is placed in the center of the TREAT core. Pulse type transients are initiated in TREAT by bringing the reactor to a low steady state power of 50 watts and then rapidly removing transient control rods, thereby resulting in a step insertion of excess reactivity. TREAT pulses initially have a Gaussian shape followed by a decaying exponential tail. Larger step reactivity insertions result in transient pulses that have higher peak powers, higher overall energy releases, and shorter pulse widths. TREAT has the ability to rapidly reinsert the transient control rods and shorten the natural transient. Clipping the transient in this fashion has the ability to reduce both the FWHM and total energy deposited. As an example, for a 4.2% $\Delta k/k$ reactivity insertion, clipping has been shown to decrease the maximum energy released from the reactor from ~2500 MJ to as low as 643 MJ and shorten the pulse width from > 100 ms to 89 ms [39]. The effect of clipping is shown in Figure 6. Because of TREAT's low starting power levels, initial changes in power are small even for very short reactor periods. As a result, the rapidly ejected transient rods are fully withdrawn from the core and resting at zero velocity before reactor power reaches appreciable levels, while clipping is triggered by a predetermined time delay in the transient programming. This approach gives the ability to tailor transients to a desired duration and energy release; however, the energy and duration are not independent parameters. The response is limited by the speed of the rod drive system (e.g., ~355 cm/s). For TREAT's 1.2 m reactor length, it takes ~280 ms for the control rods to fully

insert themselves. The current capabilities of the TREAT facility make getting truly prototypic pulse widths for RIAs in PWRs at zero power conditions (approximately 30 ms) just out of reach. However, future plant modifications involving a He-3 clipping system are under investigations and are predicted to be able to achieve pulse widths as low as 45 ms [40].

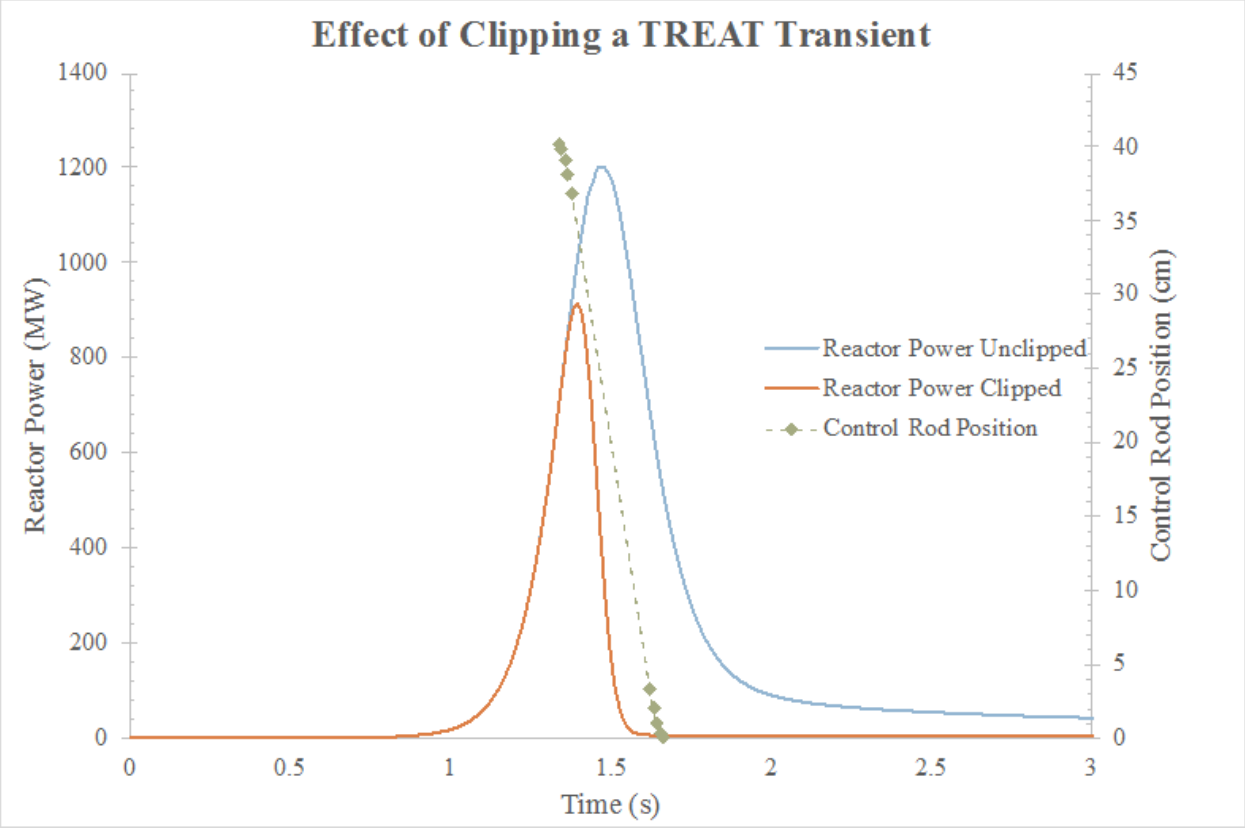

Figure 4. How clipping is used to shape TREAT's natural transients.

The first ATF transient tests occurred in July 2019 and involved the two rodlets with U_3Si_2 fuel and zircaloy-4 cladding (e.g., SETH-F and SETH-G). SETH-F underwent two transients, the first of which confirmed the expected core-to-specimen energy coupling factor of 0.44 J/g-MJ (J/g of specimen energy per MJ of TREAT reactor energy). The purpose of the second was to explore the behavior of U_3Si_2 fuel at an energy deposition slightly above the

melting enthalpies. The SETH-G transient was tested at an even more aggressive transient to determine if changes in coolable geometry could be induced when pellet enthalpies significantly above the melting point occurred. The transients with the SiC-SiC clad rodlets (e.g., SETH-H and SETH-I) took place later in October and November 2019. The purpose of SETH-H was to explore molten U_3Si_2 interactions with SiC. The purpose of SETH-I was to explore pellet cladding interactions between a still solid U_3Si_2 fuel pellet and the SiC cladding. Figure 7 shows the reactor transients for each of the five tests, while Table 2 shows rodlet test conditions for each test. Following irradiation, test capsules were shipped to INL gloveboxes for disassembly and post-transient examinations.

Table 2. TREAT transient testing conditions for ATF experiments.

Transient	Rodlet	Reactor Energy Released (MJ)	Pulse Width (ms)	Rodlet Energy Deposited (J/g)
SETH F-1	SETH F	580	100	255
SETH F-2	SETH F	900	100	396
SETH-G	SETH G	1200	95	528
SETH-H	SETH H	1200	95	528
SETH-I	SETH I	750	100	330

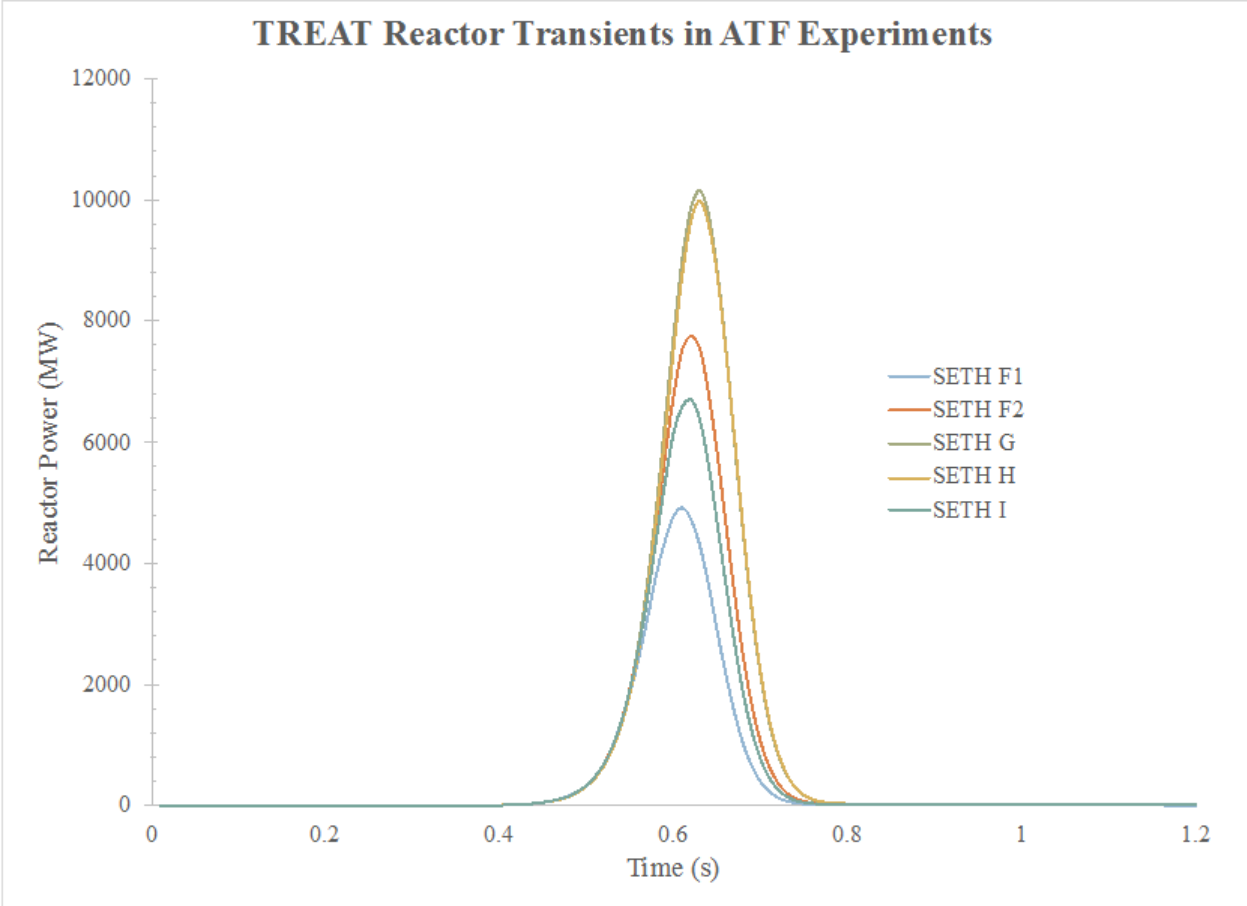

Figure 5. TREAT power transients during ATF experiments.

3 Experiment Calculations

Fuel performance simulations of the transients were made using the BISON fuel performance code [41]. The purpose of the simulations was to calculate a first order approximation of fuel and cladding temperatures during each test to determine the extent of fuel melting as well as to evaluate first order approximation of PCI induced stresses in the SiC-SiC cladding during the SETH-I test. The modelling work is intentionally simplistic in this case as the appropriate material properties/models (U_3Si_2 heat of fusion, specific volume change upon melting, etc.) to assess the fuel behavior post melting are not available.

Three axisymmetric meshes were constructed for each of the three rodlet geometries (e.g., zircaloy-4 clad, SiC-SiC clad with large gap, and SiC-SiC clad with small gap). The mesh used first order quadrilinear finite elements. Ten elements were used across the pellet radius and five elements were used across the cladding thickness; the axial node density was selected to maintain an aspect ratio of greater than 3:1. Cladding endcap features where not explicitly modeled but mesh volume was chosen to conserve the mass between the model and test rod as this has a significant impact on the predicted temperatures during the transient heat transfer calculation. The transient power distribution in the fuel was assumed to be uniform as radial peaking should be limited in the fresh fuel case. The outer SiC monolith layer that is typically found in SiC-SiC cladding architectures was also not explicitly modeled. Non-frictional contact was used on the fuel cladding interface and a constant gap conductivity of 0.15 W/mK was used to model the thermal conductivity of the helium-filled gap. While the thermal conductivity of helium does increase with temperature (0.225 W/mK at 315 C) it was determined that this change would have a negligible effect of the results given the inherent limitations of the model at calculating temperatures past the fuel melting point. An empirically derived heat transfer coefficient was used on the cladding outer diameter. The correlation was empirically determined from previous experiments in the SETH capsule with zircaloy cladding. The correlation is developed by performing a heat balance on the fuel pins using temperature decay data from the pyrometers and thermocouples. In deriving the correlation, only temperature decay data from ~10 seconds after the transient is used when it can be reasonably assumed that no heat is being added to the fuel pin and that changes in temperature with respect to time are dominated by heat loss from the cladding surface. This correlation is shown in equation (1). T-infinity was assumed to be 300 K in the calculation. It is acknowledged that use of this equation in the SiC-SiC clad tests is suspect due to differences in material emissivity. However, previous analysis of RIA

transients in the SETH capsule has shown that for prompt clipped transients, peak fuel temperatures and even peak cladding temperatures are relatively insensitive over a wide range of heat transfer conditions on the cladding surface [42]. Differences in measured and predicted cladding temperatures later in the transient are expected to be more significant. However, as the purpose of the model was to evaluate peak fuel and cladding temperatures early in the transient it was determined that use of this correlation would be adequate.

(1)

The U_3Si_2 fuel was modeled in a linear elastic fashion. The density of the material was modeled as 94% theoretical density or 11.47 g/cm^3 consistent with the density of the as fabricated pellets. The linear coefficient of thermal expansion was modeled as 1.6×10^{-5} K^{-1}. Other thermophysical properties used in the analysis include heat capacity and thermal conductivity as a function of temperature shown in equations (2) and (3), which are valid until 1775 K. Mechanical properties for the fuel included a Young's modulus of 140 MPa and a Poisson's ratio of 0.17. These values are taken from the U_3Si_2 material property handbook [43]

(2)

(3)

The zircaloy cladding was also modeled in a linear elastic fashion. The density of the cladding taken as 6.5 g/cm^3. The linear coefficient of thermal expansion was set at a constant of 1.3×10^{-5} K^{-1}. Young's modulus was taken to be 75 MPa and Poisson's ratio was set at 0.3. Thermal conductivity as a function of temperature is shown in equation (4) and heat capacity as a function of temperature was interpolated between values in Table 3 [44].

(4)

Table 3. Heat capacity of zircaloy metal.

Temperature (K)	Specific Heat Capacity (J/kg-K)
300	281
400	302
640	331
1090	375
1093	502
1113	590
1133	615
1153	719
1173	816
1193	770
1213	619
1233	469
1248	356

The SiC-SiC cladding was modeled with a Young's modulus of 200 MPa and Poisson's ratio of 0.3 in the elastic regime. The cladding proportional limit stress, which is analogous to the yield stress, was set at 150 MPa. A post yield hardening coefficient of 36.4 MPa was then used to determine the cladding stress after the proportional limit stress was reached [18]. Thermophysical properties for SiC used in the model are functions of temperature and are described in equations (5), (6), and (7) [45][46].

(5)

(6)

(7)

Results of the BISON model with the SiC-SiC rodlet used in SETH-I show that for a 330 J/g transient, pellet cladding mechanical contact does take place prior to the pellet melting. This contact occurs when the pellet centerline temperature is at 1150°C and the pellet surface temperature is at 640°C. The model shows that initially the cladding outer diameter (OD)

experiences a tensile hoop stress, while the inner diameter (ID) experiences a compressive hoop stress due to thermal stress gradients as the rod heats up. When the fuel pellet contacts the cladding, the stress state in the cladding ID reverses and becomes tensile with a peak value of 25 MPa. The model shows that the cladding reaches a peak hoop stress on the OD of 190 MPa and a peak hoop strain of 0.32%. These values are beyond the proportional limit stress but below the ultimate tensile stress limit. These conditions should be sufficient to initiate cracking in the outer surface of the cladding. Model predictions of cladding stress in SETH-I are shown in Figure 8. The model predictions of cladding and fuel temperature for all the transients are shown along with the measured results of cladding temperature from the thermocouples and pyrometers in the results section.

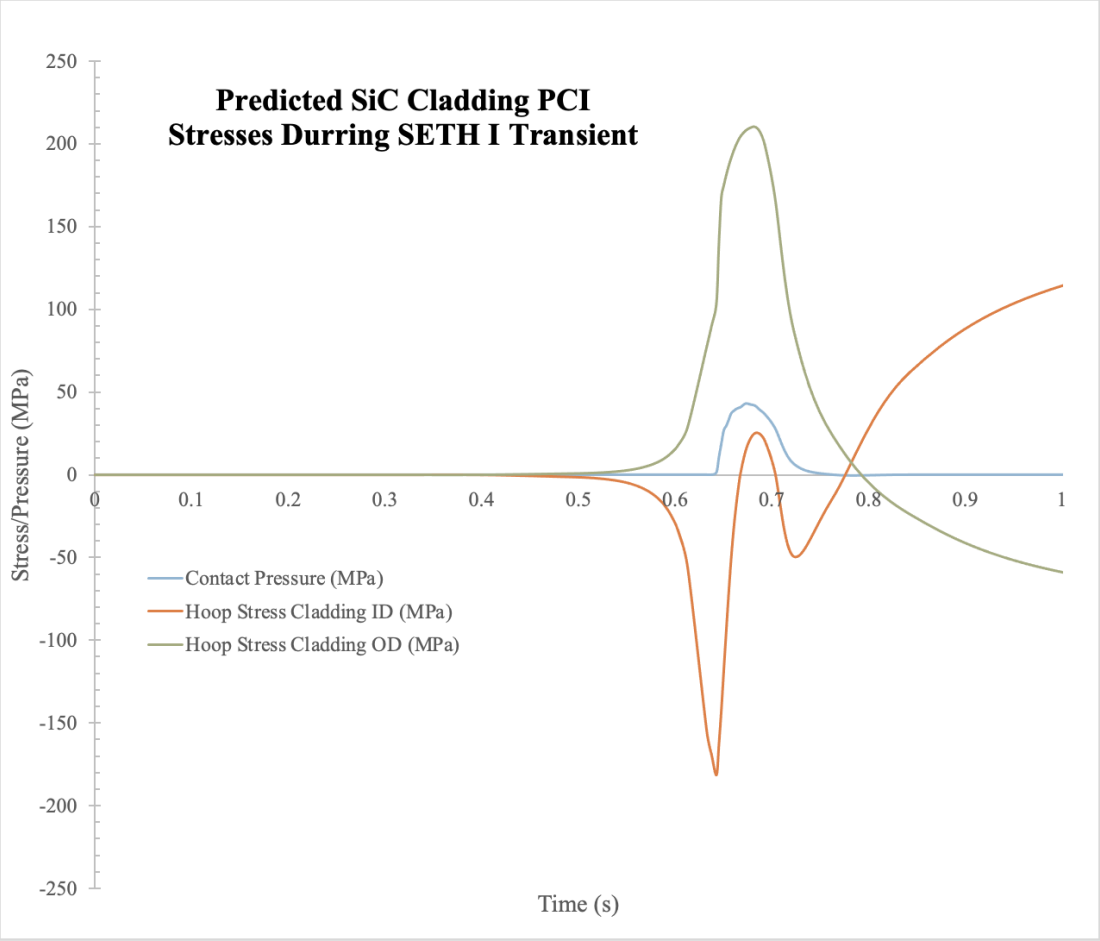

Figure 6. Calculated stress state in SiC cladding during PCI transient.

4 Results

4.1 Transient Irradiations

In the first SETH-F-1 transient, the pyrometers and para-axial cladding thermocouples responded similarly with peak cladding temperatures occurring between 3 and 4 seconds after the transient between 740°C and 770°C. The perpendicular thermocouples responded slower and had lower temperatures due to an increase in the thermocouple "fin" affect in combination with the physical location of the junction being further away from the cladding. The peak temperatures were much lower than those predicted by the BISON model, which predicted peak temperatures of 855°C at 3 seconds after the transient. Temperature measurements and model predictions for SETH-F1 are shown in Figure 9.

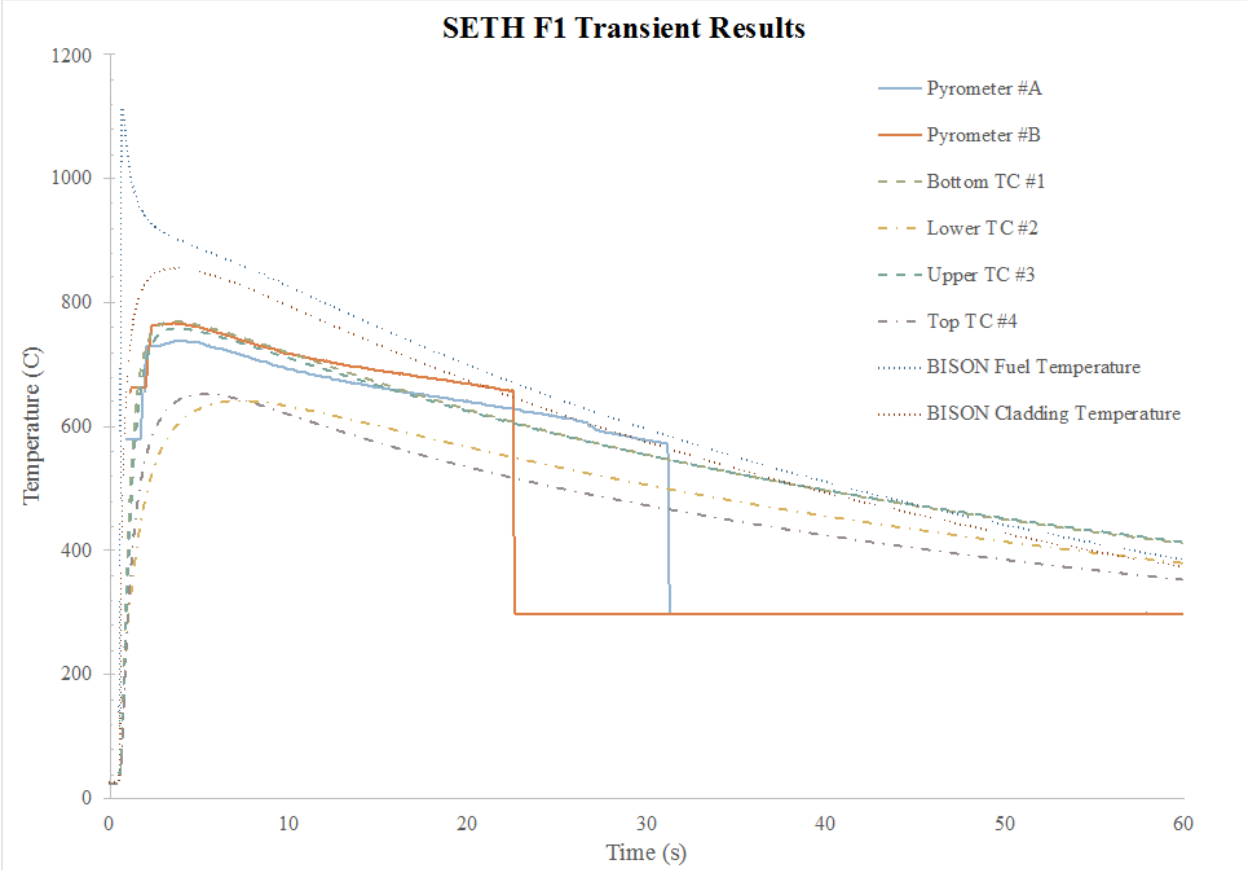

Figure 7. SETH-F-1 transient temperatures.

In the second transient, SETH-F-2, there was a more pronounced difference between the temperatures recorded by the pyrometer and those of the thermocouple. The transient released 50% more energy than the first SETH-F-1 so the temperatures were much higher. The pyrometers reported peak cladding temperatures between 1225°C and 1265°C between 2.5 and 3.5 seconds, respectively. These values were closer to the BISON model prediction of 1315°C at 2.3 seconds into the transient. The para-axial thermocouples reported lower peak cladding temperatures of 1073°C, while the perpendicular thermocouples were even lower still with peak cladding temperatures between 900°C and 940°C. Temperature measurements and model predictions for SETH-F-2 are shown in Figure 10.

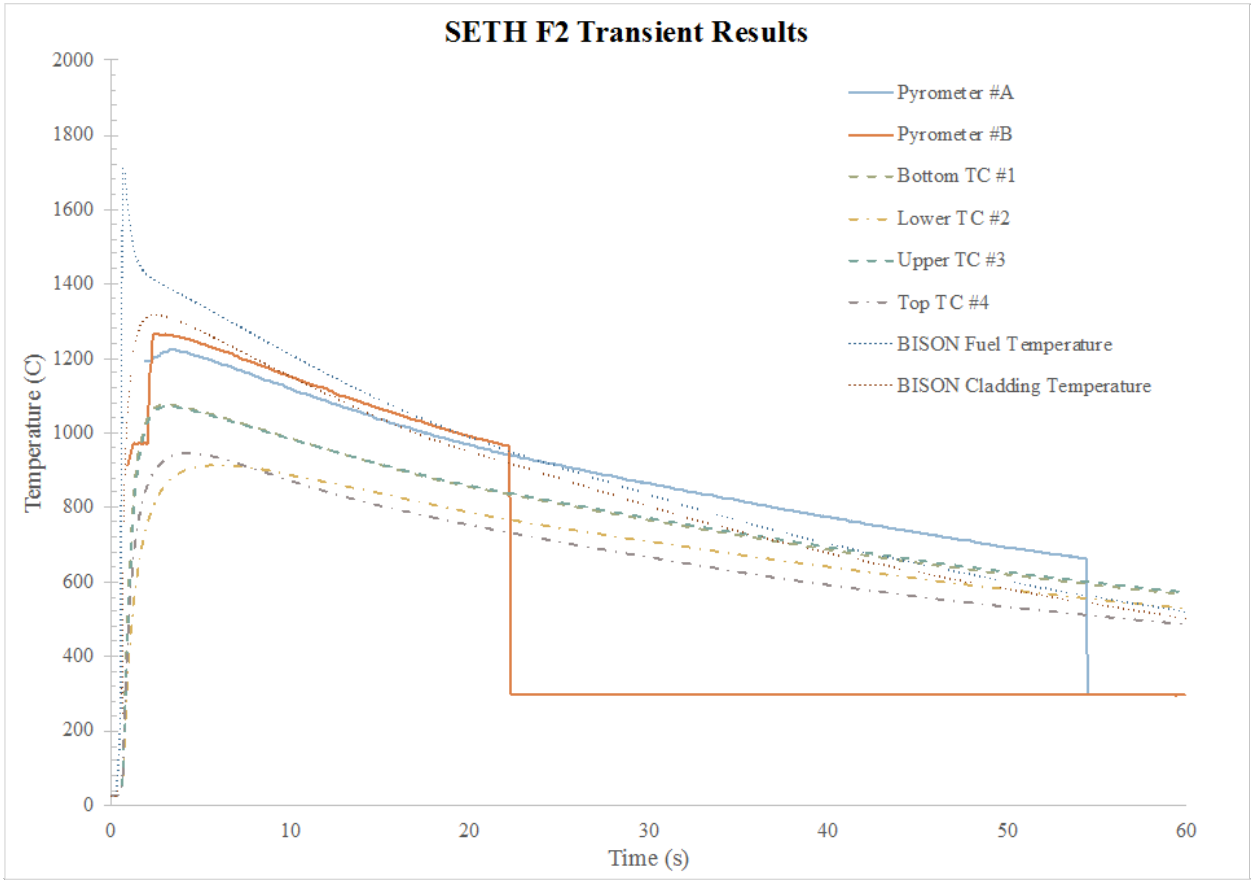

Figure 8. SETH-F-2 transient temperatures.

The SETH-G transient had the highest energy release and resulted in the highest cladding temperatures. As with SETH-F-2, there was significant variation between the pyrometer temperatures and the thermocouples—all four of which are para-axially configured in SETH-G. In SETH-G, the two pyrometer measurements agree very well with each other, as do the four para-axial thermocouples. Peak cladding temperatures from the pyrometers occur almost immediately between 1.5 and 2 seconds into the transient between 1632°C and 1640°C. These correspond very well with the BISON model, which predicted a peak temperature of 1635°C 2.5 seconds into the transient. However, the BISON model is highly suspect in this case as the thermal properties of U_3Si_2 past its melting point (e.g., 1665°C) are not known and extrapolated

from those known for the solid material in the BISON model. The top thermocouple shows a temperature spike of 100°C at 7.6 seconds. Temperature measurements and model predictions for SETH-G are provided in Figure 11.

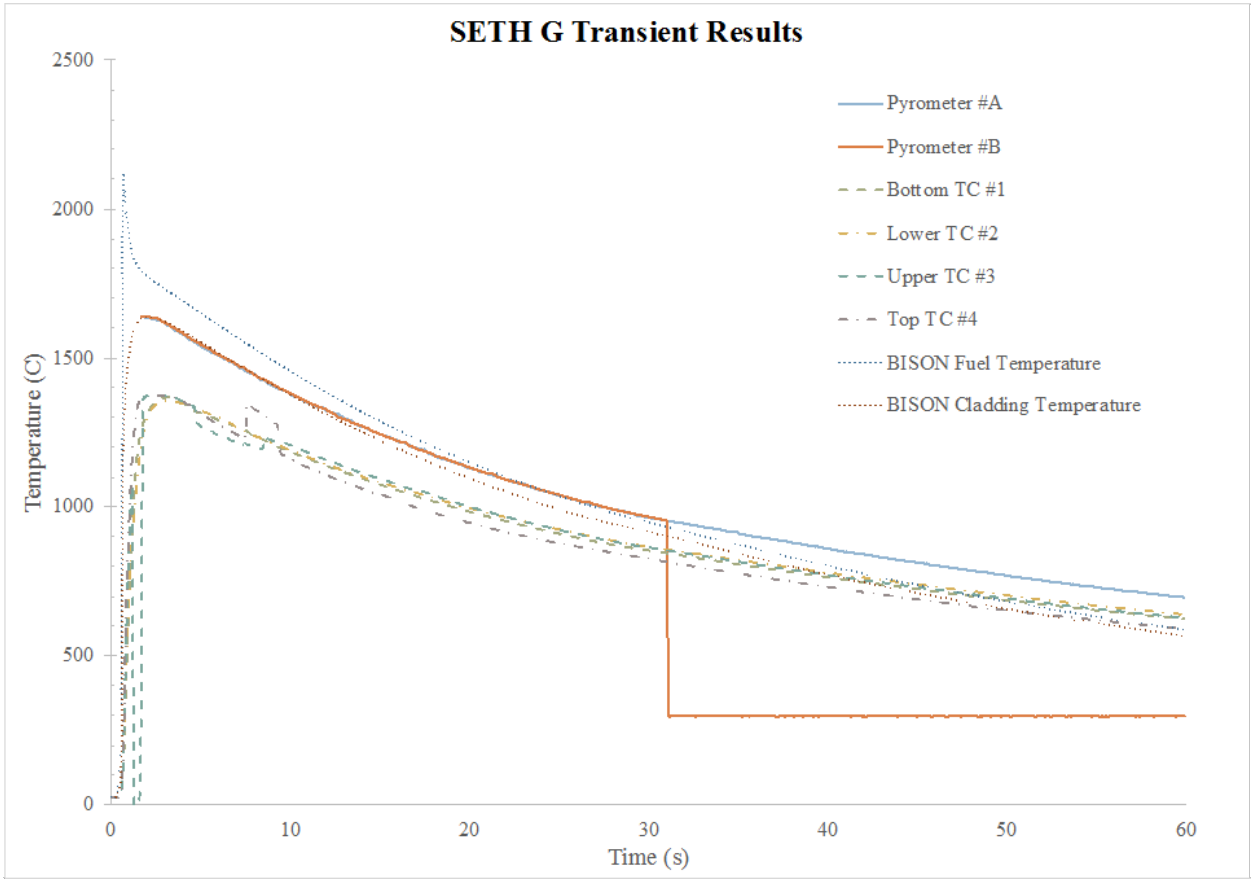

Figure 9. SETH-G transient temperatures.

The SETH-H transient was the nuclear equivalent of SETH-G; however, it took place with a SiC-SiC clad fuel rod with a large pellet cladding gap. Peak cladding temperatures were lower primarily due to the higher thermal mass of the SiC cladding and the lower thermal mass of the smaller U_3Si_2 pellets. The pyrometers recorded peak temperatures between 1133°C and 1156°C between 3 and 3.5 seconds into the transient. These temperatures were about 100 degrees

lower than those predicted by the BISON model, which predicted a temperature of 1249°C at nearly 4 seconds into the transient. The thermocouples all responded much slower with lower peak temperatures arising from higher contact resistance to the SiC due to the attachment methods. Temperature measurements and model predictions for SETH-H are shown in Figure 12.

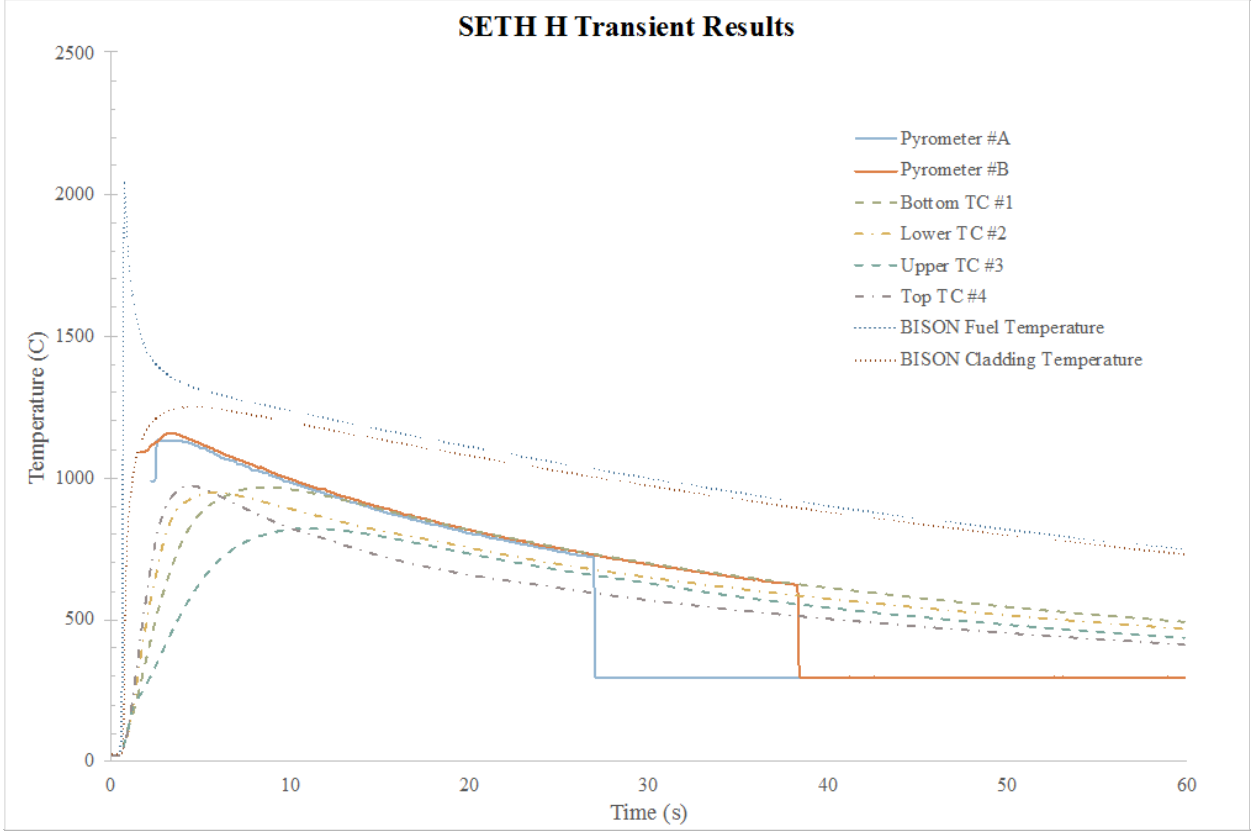

Figure 10. SETH-H transient temperatures.

As described above, the purpose of the SETH-I test was to investigate PCI behavior with SiC-SiC cladding with limited or zero fuel melting. As such, the magnitude of the SETH-I transient was significantly lower. The PCI event was predicted to take place between 0.5 and 1 second after the transient in the BISON model. Peak cladding temperatures occurred later

between 3 and 4 seconds after the transient and were recorded as 831°C and 840°C on the pyrometer. The BISON model predicted peak temperatures near 900°C at 4 seconds into the transient. Thermocouple temperatures varied greatly but were in general lower and slower than the pyrometers and BISON model predictions. Temperature measurements and model predictions for SETH-I are shown in Figure 13.

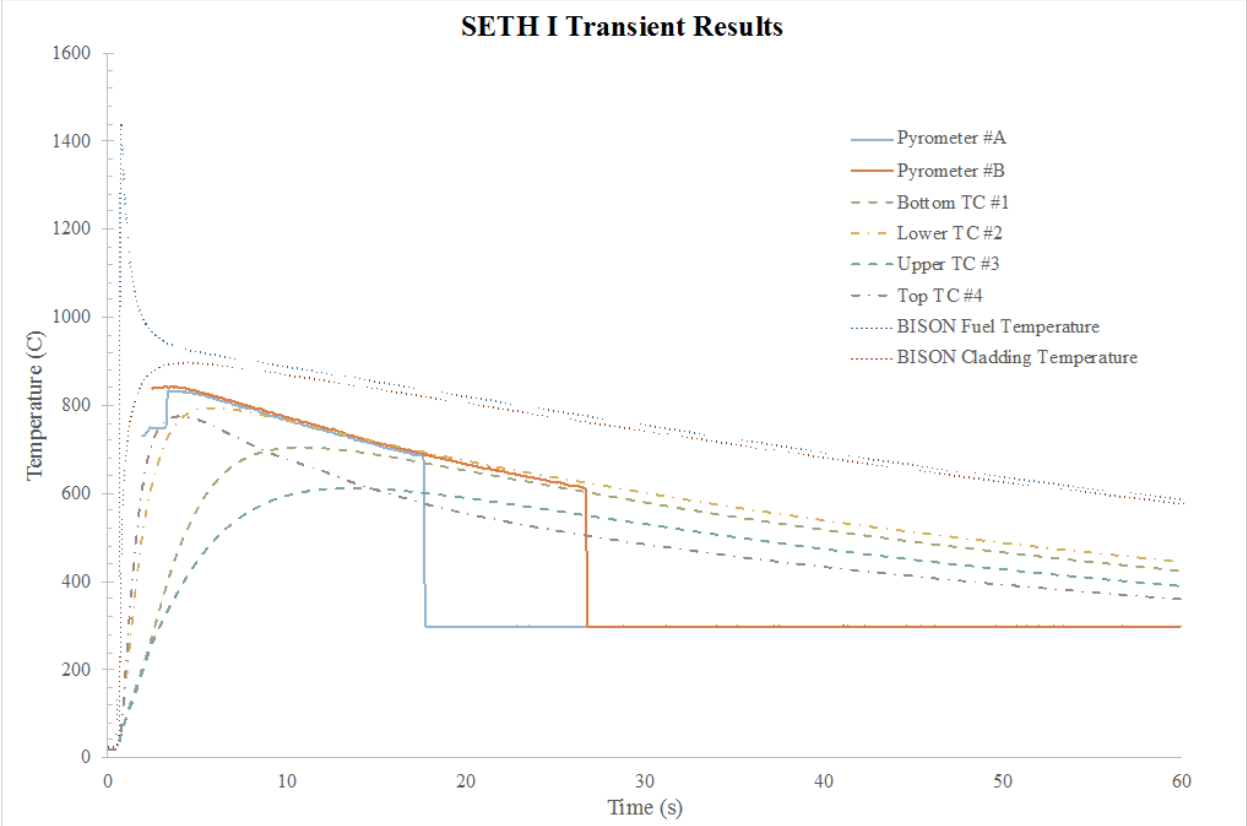

Figure 11. SETH-I transient temperatures.

4.2 Post-Transient Examinations

Following the transient tests, the SETH capsules containing the fuel test specimens were transferred from TREAT to the Materials and Fuels Complex (MFC), also located at INL, for disassembly and post-transient examination. Care is taken to minimize handling and best preserve the geometric configuration of the test. Capsules are disassembled in a shielded nitrogen

gas atmosphere glovebox to minimize oxidation and further degradation of the materials. Height restrictions in the glovebox necessitate that the capsule internals are extracted in the horizontal orientation. Visual examination is performed through the glovebox wall/window with an optical camera with no image magnification. Diameter measurements of the rodlets were performed using a micrometer. After the non-destructive visual and dimensional inspections were performed, the rodlets were sectioned and mounted for subsequent microstructural analysis, which is currently in process and will be reported separately.

SETH-F and SETH-G rodlets both retain their "rod like" geometry and appear to be free of any defects or cladding breaches. The energy depositions in those tests should have been sufficiently high enough to cause melting of the fuel. However, based on initial visual inspections this does not appear to have damaged the cladding. As none of the cladding temperature measurements are above the melting temperature of U_3Si_2 it is likely that fuel melting was confined to the central region of the fuel pellet. This could also be an indication that U_3Si_2 has a relatively high heat of fusion as particularly in the SETH-G transient much more extensive melting behavior was predicted to occur based on a comparison of enthalpy required to reach melting (350 J/g) and the amount of energy deposited in the test (528 J/g). Post transient visuals of SETH-F and SETH-G are shown in Figure 14 and Figure 15, respectively.

Additionally, the expected fuel melting behavior did not seem to impact the SiC-SiC clad rodlet, SETH-H, as it appears to maintain its geometry as well and is free of any macroscale defects or macroscale cracks, as observed in Figure 16. The SETH-I rodlet does appear to have an unidentified defect on the outside of the cladding, as seen in Figure 17. The defect appears to be a small circumferential crack extending approximately 30-45 degrees with noticeable burn marks around the crack. However, the defect is less severe than those seen during cladding

breeches involving zircaloy cladding during sever transients, which are typically characterized by either a long axial crack as the result of PCI fracture or a balloon and burst as the result of prolonged high temperature excursions [5]. The crack is also not typical of those seen in modified burst tests which simulate failure due to PCMI [31]. Post-transient profilometry did not identify any significant ballooning or collapsing of the cladding with all measurements being within 0.25% of the nominal diameter of 9.5 mm. While all the experiments maintained a "rod-like" geometry it could not be determined if any microscale cladding breaches occurred by simple visual inspection. Later planned destructive examinations will determine the presence and extent of any micro-cracking and/or loss of hermiticity in the fuel rod.

Figure 12. Post-transient visual examination of SETH-F rodlet.

Figure 13. Post-transient visual examination of SETH-G rodlet.

Figure 14. Post-transient visual examination of SETH-H rodlet.

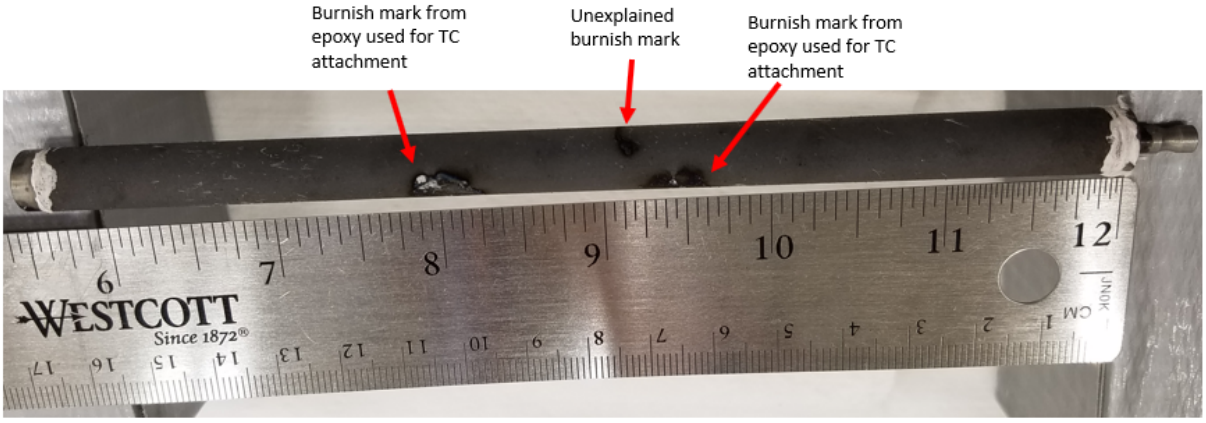

Figure 15. Post-transient visual examination of SETH-I rodlet.

5 Discussion

Nuclear fuel safety criteria for RIA events are generally reported in terms of a peak radial average enthalpy or a change in peak radial average enthalpy. Limits are designated for maintenance of core coolability as well as lower limits for fuel system failure which is generally interpreted as cladding rupture. For the current LWR fuel design, the initial enthalpy limit for fuel rods consisting of UO_2 pellets incased in a zircaloy cladding were established in 1974 and published in Atomic Energy Commission (AEC) Regulatory Guide 1.77 [47]. Initially, a core coolability limit was set to 1170 J/g-UO_2 radial average fuel enthalpy for both fresh and

irradiated fuel based on the maintenance of rod-like (e.g., coolable) geometry. This enthalpy limit was based on a review of SPERT and TREAT experimental data from the 1960s. Later studies during the RIA program performed at PBF highlighted a discrepancy between total energy deposited and peak enthalpy in transient irradiations and terminology used in the regulatory guide [48]. The reactor coolability criteria was thus adjusted and is now set at 962 J/g-UO_2 peak radial average enthalpy for LWR fuel consisting of UO_2 fuel pellets in a zircaloy cladding [49]. Cladding failure limits are generally much less than this, and for high burnup rods, can be as low at 209 J/g based on hydrogen content of the Zircaloy claddings [50].

While the test set is limited and the environment not prototypic, these results indicate that RIA enthalpy limits based on maintenance of coolable geometry for fuel rods consisting of U_3Si_2 fuel in zircaloy cladding or SiC-SiC cladding, could start as high as 528 J/g-U_3Si_2 for fresh fuel. The helium environment in SETH is conservative when assessing peak cladding temperatures and failure modes due to melting, however it may be nonconservative when the effects of high temperature oxidation and quench loads are considered. More experiments would certainly be required to verify or extend this limit including tests done in a more prototypic pressurized water environment. RIA limits will also need to be re-examined for the fuel as its burnup increases.

6 Conclusion

The restart of the TREAT reactor at INL provides the opportunity to gather new experimental data on the behavior of novel fuel and cladding materials in transient RIA conditions. The first such tests were recently performed using Uranium Silicide fuel in both zircaloy and Silicon Carbide composite cladding which are currently being proposed as ATF concepts. These initial tests indicate that these ATF designs maybe able to withstand energy depositions that induce some localized fuel melting and still maintain a “rod-like” or coolable

geometry.

7 Acknowledgements

This work was supported through the U.S. Department of Energy Advanced Fuels Campaign under DOE Idaho Operations Office Contract DE-AC07-05ID14517. Accordingly, the U.S. Government retains and the publisher, by accepting the article for publication, acknowledges that the U.S. Government retains a nonexclusive, paid-up, irrevocable, world-wide license to publish or reproduce the published form of this manuscript, or allow others to do so, for U.S. Government purposes.

8 Declaration of Interest

References

1 United States Department of Energy, *Development of Light Water Reactor Fuels with Enhanced Accident Tolerance Report to Congress,* Washington, D.C., USA (2015).

2 Cappia F., Harp J.M., "Postirradiation examinations of low burnup U_3Si_2 fuel for light water reactor applications" *Journal of Nuclear Materials,* Vol 518 (2019)

3 Sweet R.T., Yang Y., Terrani K.A., Wirth B.D., Nelson A.T., "Performance of U_3Si_2 in an LWR following a cladding break during normal operation" *Journal of Nuclear Materials,* Vol 539 (2020)

4 Nelson A.T., Migdisov A., Sooby Wood E., Grote C.J., "U_3Si_2 behavior in H_2O environments: Part II, pressurized water with controlled redox chemistry" *Journal of Nuclear Materials,* Vol 500 (2018)

5 Nuclear Energy Agency *State of the Art Report on Light Water Reactor Accident Tolerant Fuels* NEA No. 7317 (2018)

6 Doyle P.J. Ang C., Snead L., Katoh Y., Terrani K., Raiman S., "Hydrothermal Corrosion of First-Generation Dual-Purpose Coatings on Silicon Carbide for Accident-Tolerant Fuel Cladding" *Journal of Nuclear Materials* Vol 544 (2021)

7 Koyanagi T., Katoh Y., Nozawa T., "Design and strategy for next-generation silicon carbide composites for nuclear energy" *Journal of Nuclear Materials* Vol 540 (2020)

8 Petrie C.M., Koyanagi T., McDuffee J.L., Deck C.P., Katoh Y., Terrani K.A., "Experimental design and analysis for irradiation of SiC/SiC composite tubes under a prototypic high heat flux" *Journal of Nuclear Materials* Vol 491 (2017)

9 Stone J.G., Schleicher R., Deck C.P., Jacobsen G.M., Khalifa H.E., Back C.A., "Stress analysis and probabilistic assessment of multi-layer SiC-based accident tolerant nuclear fuel cladding," *Journal of Nuclear Materials*, Vol 466 (2015).

10 Li W., Shirvan K., "U_3Si_2-SiC fuel performance analysis in BISON during normal operation" *Annals of Nuclear Energy* Vol. 132 (2019)

11 He Y., Shirvan K., Wu Y., Su G.H., "Fuel Performance optimization of U_3Si_2-SiC design during normal, power ramp, and RIA Conditions" *Nuclear Engineering and Design* Vol 353 (2019)

12 Nuclear Energy Agency Working Group on Fuel Safety, *Nuclear Fuel Behavior Under Reactivity-initiated Accident Conditions State of the Art Report*, NEA No. 6847 (2010).

13 Grigoriev V., Jakobsson R., Shrire D., Ledergerber G., Surgiyama T., Nagase F., Fuketa T., Hallstadius L., Valizadeh S., "RIA failure of high burnup fuel rod irradiated in the Leibstadt reactor: Out-of-pile mechanical simulation and comparison with pulse reactor tests," *Journal of ASTM International*, Vol. 7, No. 9 (2010).

14 Papin J., Cazalis B., Frizonnet M., Desquines J., Lemoine F., Geogenthum V., Lamare F., Petit M., "Summary and interpretation of the CABRI REP-Na program," *Nuclear Technology*, Vol 157, No 3 (2017).

15 Nyer W.E., Forbes S.G., *SPERT Program Review*, IDO-16634 (1960).

16 McCardell R.K., MacDonald P.E., "Safety and licensing issues that are being addressed

by the Power Burst Facility test programs," *CSNI Specialist Meeting on Safety Aspects of Fuel Behavior in Off-Normal and Accident Conditions*, Helsinki, Finland (1980).

17 Jensen C.J., Woolstenhulme N.E., Wachs D.M., "The TREAT experiment legacy supporting LWR fuel technology," *Proceedings TopFuel 2018*, Prague, Czech Republic (2018).

18 Woolstenhulme N., Baker C., Bess J., Chapman D., Dempsey D., Hill C., Jensen C., Snow S., "New capabilities for in-pile separate effects tests in TREAT," *Proceedings from ANS Annual Meeting* (2018).

19 Woolstenhulme N., Fleming A., Holschuh T., Jensen C., Kamerman D., Wachs D., "Core-to-specimen energy coupling results of the first modern fueled experiments in TREAT," *Annals of Nuclear Energy*, Vol 140 (2020).

20 Schulthess J., Woolstenhulme N., Craft A., Kane J., Boulton N., Chuirazzi W., Winston A., Smolinski A., Jensen C., Kamerman, D., Wachs D., "Non-destructive post-irradiation examination results of the first modern fueled experiments in TREAT," *Journal of Nuclear Materials* Vol 541 (2020).

21 Wagner A.R., Harp J.M., Archibald K.E., Ashby S.C., Watkins J.K., Tolman K.R., "Fabrication of stoichiometric U_3Si_2 fuel pellets," *MethodsX*, Vol 6 (2019).

22 Harp J M., Lessing P.A., Hoggan R.E., "Uranium silicide pellet fabrication by powder metallurgy for accident tolerant fuel evaluation and irradiation," *Journal of Nuclear Materials*, Vol 466 (2015).

23 Shapovalov K., Jacobsen G.M., Shih C., Deck C.P., "C-ring testing of nuclear grade silicon carbide composites at temperatures up to 1900 C," *Journal of Nuclear Materials*, Vol 522 (2019).

24 Berche A., Rado C., Rapaud O., Gueneau C., Rogez J., "Thermodynamic study of the U-Si system" *Journal of Nuclear Materials* Vol 389 (2009)

25 White J.T., Nelson A.T., Dunwoody J.T., Byler D.D., Safarik D.J., McClellan K.J., "Thermophysical properties of U_3Si_2 to 1773K," *Journal of Nuclear Materials*, Vol 464 (2015).

26 International Atomic Energy Agency, *Thermophysical properties database of materials for light water reactors and heavy water reactors*, IAEA-TECDOC-1496, Vienna, Austria (2006).

27 Lemaignan C., "2.07 Zirconium Alloys: Properties and Characteristics," *Comprehensive Nuclear Materials* (2012).

28 Jacobsen G., Chiger H., *Product Engineering Nuclear Materials Property Manual General Atomics Silicon Carbide Cladding*, GA-A28712 (2017).

29 Price R.J., "Thermal Conductivity of Neutron-Irradiated Pyrolytic β-Silicond Carbide" *Journal of Nuclear Materials* Vol 46 (1973)

30 Katoh Y., Ozawa K., Shih C., Nozawa T., Shinavski R.J., Hasegawa A., Snead L.L., "Continuous SiC fiber, SVI SIC matrix composites for nuclear applications: Properties and irradiation effects" *Journal of Nuclear Materials* Vol 448 (2014)

31 Cinbiz M.N., Koyanagi T., Singh G., Katoh Y., Terrani K.A., Brown N.R., "Failure

behavior of SiC/SiC composite tubes under strain rates similar to the pellet-cladding mechanical interaction phase of reactivity-initiated accidents" *Journal of Nuclear Materials* Vol 514 (2019)

32 Yingling J.A., Gamble K.A., Roberts E., Freeman R.A., Knight T.W., "UPDATED U3Si2 thermal creep model and sensitivity analysis of the U3Si2-SIC accident tolerant FUEL" *Journal of Nuclear Materials* Vol 543 (2021)

33 Deck C.P., Jacobsen G.M., Sheeder J., Gutierrez O., Zhang J., Stone J., Khalifa H.E., Back C.A., "Characterization of SiC-SiC composites for accident tolerant fuel cladding," *Journal of Nuclear Materials*, Vol 466 (2015).

34 Jensen C., Flemming A., "Development of advanced instrumentation for transient testing," *Nuclear Technology*, Vol 205 (2019).

35 B. Bouvry, G. Cheymol, L. Ramiandriosa, B. Javaudin, C. Gallou, H. Maskrot, N. Horny, T. Duvaut, C Destouches, L. Ferry, C. Gonnier, "Multispectral pyrometry for surface temperature measurement of oxidized Zircaloy claddings." *Infrared Physics and Technology* Vol 83, (2017)

36 Silicon Carbide, SiC, Normal Spectral Emittance, Retrieved from CINDAS LLC Thermophysical Properties of Matter Database (TPMD). Version 10.0 accessed at <http://cindasdata.com/>

37 Woolstenhulme N., Baker C., Jensen C., Chapman D., Imholte D., Oldham N., Hill C., Snow S., "Development of irradiation test devices for transient testing," *Nuclear Technology*, Vol 205 (2019).

38 Pope C.L., Jensen C.B., Gerstner D.M., Perry J.R., "Transient Reactor Test (TREAT) facility design and experiment capability," *Nuclear Technology*, Vol 205 (2019).

39 Holschuh T., Woolstenhulme N., Baker B., Bess J., Davis C., Parry J., "Transient Reactor Test facility advanced ttransient shapes," *Nuclear Techonology*, Vol 205 (2019).

40 Bess J.D., Woolstenhulme N.E., Davis C.B., Dusanter L.M., Folsom C.P., Parry J.R., Shorthill T.H., Zhao H., "Narrowing transient testing pulse widths to enhance LWR RIA experiment design in the TREAT facility," *Annals of Nuclear Energy*, Vol. 124 (2019).

41 Williamson R.L., Hales J.D., Novascone S.R., Tonks M.R., Gaston D.R., Permann C.J., Andrs D., Martineau R.C., "Multidimensional multiphysics simulation of nuclear fuel behavior," *Journal of Nuclear Materials*, Vol 423 (2012).

42 Kamerman D., Woolstenhulme N., Jensen C., Wachs D., "BISON Fuel Performance Simulations of TREAT Transients" *Proceedings ANS 2019 Annual Meeting* Minneapolis MN (2019)

43 White J.T., *U_3Si_2 Fuel Property Handbook*, LA-UR-18-28719 (2018).

44 Idaho National Engineering and Environmental Laboratory, *MATPRO – A Library of Materials Properties for Light-Water-Reactor Accident Analysis*, NUREG/CR-6150 (2001).

45 Koyanagi T., Katoh Y., Singh G., Snead M., *SiC/SiC Cladding Materials Properties Handbook*, ORNL/TM-2017/385 Oak Ridge National Laboratory (2017).

46 Snead L.L., Nozawa T., Katoh Y., Byun T.-S., Kondo S., Petti D.A., "Handbook of Sic

properties for fuel performance modeling," *Journal of Nuclear Materials*, Vol 317 (2007).

47 U.S. Atomic Energy Commission, "Regulatory Guide 1.77," May 1974, pp. 1–8 (1974).

48 P. E. MacDonald, "Assessment of Light Water Reactor Fuel Damage During a Reactivity Initiated Accident," *CSNI Specialist Meeting on Safety Aspects of Fuel Behavior in Off-Normal and Accident Conditions*, Helsinki, Finland (1980).

49 Nuclear Regulatory Comission, "NUREG-0800, Ch. 4.2, Rev. 3," No. 301, pp. 33–36, (2007).

50 Nuclear Regulatory Comission, "Draft Regulatory Guide DG-1327 Pressurized Water Reactor Control Rod Ejection and Boiling Water Reactor Control Rod Drop Accidents," (2016).